Article
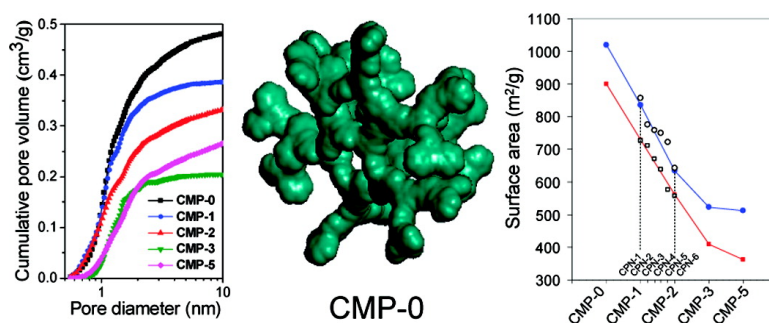
Synthetic Control of the Pore Dimension and Surface Area in Conjugated Microporous Polymer and Copolymer Networks

Jia-Xing Jiang, Fabing Su, Abbie Trewin, Colin D. Wood, Hongjun
Niu, James T. A. Jones, Yaroslav Z. Khimyak, and Andrew I. Cooper

CMP-0

More About This Article

Additional resources and features associated with this article are available within the HTML version:

- Supporting Information
- Links to the 2 articles that cite this article, as of the time of this article download
- Access to high resolution figures
- Links to articles and content related to this article
- Copyright permission to reproduce figures and/or text from this article

View the Full Text HTML

Synthetic Control of the Pore Dimension and Surface Area in Conjugated Microporous Polymer and Copolymer Networks

Jia-Xing Jiang, Fabing Su, Abbie Trewin, Colin D. Wood, Hongjun Niu,
James T. A. Jones, Yaroslav Z. Khimyak, and Andrew I. Cooper*

*Department of Chemistry and Centre for Materials Discovery, University of Liverpool,
Liverpool L69 3BX, United Kingdom*

Received February 15, 2008; E-mail: aicooper@liv.ac.uk

Abstract: A series of rigid microporous poly(aryleneethynylene) (PAE) networks was synthesized by Sonogashira−Hagihara coupling chemistry. PAEs with apparent Brunauer−Emmet−Teller surface areas of more than 1000 m²/g were produced. The materials were found to have very good chemical and thermal stability and retention of microporosity under a variety of conditions. It was shown that physical properties such as micropore size, surface area, and hydrogen uptake could be controlled in a "quantized" fashion by varying the monomer strut length, as for metal−organic and covalent organic frameworks, even though the networks were amorphous in nature. For the first time, it was demonstrated that these properties can also be fine-tuned in a continuous manner via statistical copolymerization of monomer struts with differing lengths. This provides an unprecedented degree of direct synthetic control over micropore properties in an organic network.

Introduction

Microporous materials (pore diameters <2 nm) are interesting because of their applications in areas such as molecular separations, heterogeneous catalysis, and gas storage. Significant advances have been made recently, particularly in the preparation of microporous crystalline metal−organic frameworks (MOFs)[1,2] and covalent organic frameworks (COFs).[3–6] In some cases it has been possible to tune material properties such as density, pore volume, and surface area for series of MOFs and COFs by varying the length and geometry of the rigid organic linkers.[1–6]

Organic microporous polymers possess a number of advantages. First, they can be composed solely of light elements (C, H, O, N, etc.). Second, it is possible to achieve control over functionality in organic polymers by a wide variety of synthetic strategies. Third, most organic polymers are highly stable to

air, atmospheric moisture, and, often, much more rigorous conditions. These advantages notwithstanding, there are relatively few approachs for the direct synthesis of microporous organic polymers with high specific surface areas (surface areas >1000 m²/g). Polymers of intrinsic microporosity (PIMs) can exhibit apparent Brunauer−Emmet−Teller (BET) specific surface areas of 500−1065 m²/g.[7] Hyper-cross-linked polymers (HCPs) are a class of molecularly porous organic polymer networks with BET surface areas that can exceed 2000 m²/g.[8–11] We have shown in a recent paper[12] that amorphous conjugated microporous polymers (CMPs) can be synthesized with surface areas in the range 500−800 m²/g by using Pd(0)/Cu(I)-catalyzed Sonogashira−Hagihara cross-coupling chemistry.[13] These poly-(aryleneethynylene) (PAE) materials represent the first examples

(1) (a) Yaghi, O. M.; Li, H. L.; Davis, C.; Richardson, D.; Groy, T. L. *Acc. Chem. Res.* **1998**, *31*, 474–484. (b) Cheetham, A. K.; Férey, G.; Loiseau, T. *Angew. Chem., Int. Ed.* **1999**, *38*, 3268–3292. (c) Kitagawa, S.; Kitaura, R.; Noro, S. *Angew. Chem., Int. Ed.* **2004**, *43*, 2334–2375. (d) Li, H.; Eddaoudi, M.; O'Keeffe, M.; Yaghi, O. M. *Nature* **1999**, *402*, 276–279. (e) Mellot-Draznieks, C.; Ferey, G. *Prog. Solid State Chem.* **2005**, *33*, 187–197. (f) Zhao, X. B.; Xiao, B.; Fletcher, A. J.; Thomas, K. M.; Bradshaw, D.; Rosseinsky, M. J. *Science* **2004**, *306*, 1012–1015. (g) Lin, X.; Jia, J. H.; Zhao, X. B.; Thomas, K. M.; Blake, A. J.; Walker, G. S.; Champness, N. R.; Hubberstey, P.; Schröder, M. *Angew. Chem., Int. Ed.* **2006**, *45*, 7358–7364.
(2) Eddaoudi, M.; Kim, J.; Rosi, N.; Vodak, D.; Wachter, J.; O'Keeffe, M.; Yaghi, O. M. *Science* **2002**, *295*, 469–472.
(3) Côté, A. P.; Benin, A. I.; Ockwig, N. W.; O'Keeffe, M.; Matzger, A. J.; Yaghi, O. M. *Science* **2005**, *310*, 1166–1170.
(4) El-Kaderi, H. M.; Hunt, J. R.; Mendoza-Cortes, J. L.; Côté, A. P.; Taylor, R. E.; O'Keeffe, M.; Yaghi, O. M. *Science* **2007**, *316*, 268–272.
(5) Côté, A. P.; El-Kaderi, H. M.; Furukawa, H.; Hunt, J. R.; Yaghi, O. M. *J. Am. Chem. Soc.* **2007**, *129*, 12914–12915.
(6) Mastalerz, M. *Angew. Chem., Int. Ed.* **2008**, *47*, 445–447.

(7) (a) Budd, P. M.; Ghanem, B. S.; Makhseed, S.; McKeown, N. B.; Msayib, K. J.; Tattershall, C. E. *Chem. Commun.* **2004**, 230–231. (b) McKeown, N. B.; Gahnem, B.; Msayib, K. J.; Budd, P. M.; Tattershall, C. E.; Mahmood, K.; Tan, S.; Book, D.; Langmi, H. W.; Walton, A. *Angew. Chem., Int. Ed.* **2006**, *45*, 1804–1807. (c) Ghanem, B. S.; Msayib, K. J.; McKeown, N. B.; Harris, K. D. M.; Pan, Z.; Budd, P. M.; Butler, A.; Selbie, J.; Book, D.; Walton, A. *Chem. Commun.* **2007**, 67–69. (d) Budd, P. M.; Butler, A.; Selbie, J.; Mahmood, K.; McKeown, N. B.; Ghanem, B.; Msayib, K.; Book, D.; Walton, A. *Phys. Chem. Chem. Phys.* **2007**, *9*, 1802–1808.
(8) (a) Tsyurupa, M. P.; Davankov, V. A. *React. Funct. Polym.* **2006**, *66*, 768–779. (b) Germain, J.; Hradil, J.; Fréchet, J. M. J.; Svec, F. *Chem. Mater.* **2006**, *18*, 4430–4435.
(9) Lee, J. Y.; Wood, C. D.; Bradshaw, D.; Rosseinsky, M. J.; Cooper, A. I. *Chem. Commun.* **2006**, 2670–2672.
(10) Wood, C. D.; Tan, B.; Trewin, A.; Niu, H. J.; Bradshaw, D.; Rosseinsky, M. J.; Khimyak, Y. Z.; Campbell, N. L.; Kirk, R.; Stöckel, E.; Cooper, A. I. *Chem. Mater.* **2007**, *19*, 2034–2048.
(11) Germain, J.; Fréchet, J. M. J.; Svec, F. *J. Mater. Chem.* **2007**, *17*, 4989–4997.
(12) Jiang, J. X.; Su, F.; Trewin, A.; Wood, C. D.; Campbell, N. L.; Niu, H.; Dickinson, C.; Ganin, A. Y.; Rosseinsky, M. J.; Khimyak, Y. Z.; Cooper, A. I. *Angew. Chem., Int. Ed.* **2007**, *46*, 8574–8578.
(13) Sonogashira, K.; Tohda, Y.; Hagihara, N. *Tetrahedron Lett.* **1975**, 4467–4470.

of *conjugated* microporous polymer networks with high surface area. We also showed that the micropore size distribution was controlled in these PAE networks by the rigid node−strut topology, in particular by the average strut length.[12] This suggests that extended long-range order as found in MOFs and COFs is not necessarily a prerequisite for fine control over micropore properties. This opens the door for a range of amorphous polymer materials with controlled pore dimensions.[14] Very recently, we also prepared homocoupled conjugated microporous poly(phenylenebutadiynylene)s with surface areas of 840 m²/g[15] and mesoporous poly(phenylenevinylene)s with surface areas of 761 m²/g,[16] although micropore size control in these cases was complicated by phase behavior and competing side reactions.

A number of synthetic strategies have been employed previously to produce linear,[17,18] hyperbranched,[19,20] dendritic,[21,22] and cross-linked[23] PAEs. Most soluble PAEs have incorporated flexible solubilizing alkyl or alkoxyl substituents. Such materials have been used as emissive layers in light-emitting diodes[18,20,22] and in nonlinear optics.[17] There are very few reports concerning the direct synthesis of porous PAE-type materials,[12,15] although Kobayashi et al.[19] have recently described the indirect preparation of porous pyrolytic polymers via treatment of alkyl-substituted PAE precursors at high temperatures (>350 °C).

We describe here a series of PAE networks synthesized by direct ($A_3 + B_2$) Pd-catalyzed cross-coupling polycondensation. Conjugated microporous PAEs with surface areas greater than 1000 m²/g were obtained, and the average micropore size was controlled by the molecular dimensions of the monomers. The results were rationalized using atomistic simulations of fragments of these networks. For the first time, we show that micropore size can be fine-tuned by statistical copolymerization of monomers with different strut lengths; this can be done in a continuous fashion with amorphous polymers but would be difficult to achieve in microporous crystalline solids.

Experimental Section

Chemicals. 1,3,5-Triethynylbenzene, 1,4-diethynylbenzene, 1,4-diiodobenzene, 4,4′-diiodobiphenyl, 1,3,5-tris-(4-iodophenyl)benzene, tetrakis(triphenylphosphine)palladium(0), (trimethylsilyl)acetylene, dichlorobis(triphenylphosphine)palladium(II), copper(I) iodide, other chemicals, and solvents were all purchased from ABCR, TCI, or Sigma-Aldrich and either recrystallized or used as received.

Synthesis of 4,4′-Diethynylbiphenyl Monomer. 4,4′-Diiodobiphenyl (4.06 g, 10.0 mmol) was dissolved in diethylamine (40 mL)

under a nitrogen atmosphere. Copper(I) iodide (50 mg) and dichlorobis(triphenylphosphine)palladium(II) (150 mg) were added to the mixture. (Trimethylsilyl)acetylene (1.96 g, 20.0 mmol) was added, and the mixture was heated to 50 °C for 12 h. After the mixture was cooled to room temperature, the precipitate that was formed was filtered off and washed with ether. The crude intermediate was purified by column chromatography (silica gel, light petroleum) to give 4,4′-bis[(trimethylsilyl)ethynyl]biphenyl as an intermediate. Deprotection was carried out by treatment with a mixture of MeOH (50 mL)/NaOH (50 mL, 1 M) under stirring at room temperature for 12 h. The product was isolated by evaporation of the organic solvent, extraction of the residue with ether, drying with Mg_2SO_4 overnight, and finally removal of the solvent under reduced pressure. The crude product was purified by column chromatography (silica gel, light petroleum) to give 4,4′-diethynylbiphenyl as white needlelike crystals (1.5 g, 74.2%). ¹H NMR (CDCl₃): δ (ppm) 7.57 (d, 4H), 7.52 (d, 4H), 3.13 (s, 2H). ¹³C NMR (CDCl₃): δ (ppm) 140.58, 132.94, 127.18, 121.55, 83.41, 78.08. Anal. Calcd for $C_{16}H_{10}$: C, 95.05; H, 4.95. Found: C, 94.26; H, 4.97. MS: m/z 220.11 [M + NH₄]⁺.

Synthesis of Poly(aryleneethynylene) Networks. All of the poly(aryleneethynylene) networks were synthesized by palladium-catalyzed Sonogashira−Hagihara cross-coupling polycondensation of arylethynylenes and aryl halides.[12,13] All reactions were carried out using a 1.5 M excess of the ethynyl functionality since this was found to maximize surface areas in the polymers (see the Supporting Information, Table S2). A typical experimental procedure for CMP-0 is given as follows:[24,25] 1,3,5-Triethynylbenzene (450.5 mg, 3 mmol), 1,3,5-tris(4-iodophenyl)benzene (1368 mg, 2.0 mmol), tetrakis(triphenylphosphine)palladium(0) (100 mg), and copper(I) iodide (30 mg) were dissolved in a mixture of toluene (2.5 mL) and Et₃N (2.5 mL). The reaction mixture was heated to 80 °C and stirred for 72 h under a nitrogen atmosphere to rigorously exclude oxygen and to prevent homocoupling of the alkyne monomers. The mixture was cooled to room temperature, and the precipitated network polymer was filtered and washed four times (once each) with chloroform, water, methanol, and acetone to remove any unreacted monomer or catalyst residues. Further purification of the polymers was carried out by Soxhlet extraction with methanol for 48 h. The product was dried in vacuum for 24 h at 70 °C. Yield: 67.3%. IR (KBr, cm⁻¹): 3297.6 (−C′C−H), 2201.7 (−C′C−). Anal. Calcd for $C_{36}H_{18}$: C, 95.25; H, 4.75. Found: C, 86.15; H, 4.41. Apparent BET surface area: 1018 m²/g.
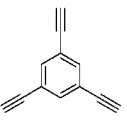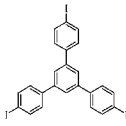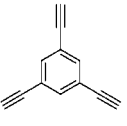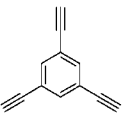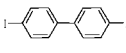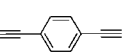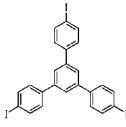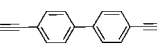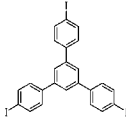
Gas Sorption Analysis. Surface areas and pore size distributions were measured by nitrogen adsorption and desorption at 77.3 K using either a Micromeritics ASAP 2420 or a Micromeritics ASAP 2020 volumetric adsorption analyzer. Samples were degassed at 110 °C for 15 h under vacuum (10⁻⁵ bar) before analysis. Hydrogen isotherms were measured at 77.3 K up to 1.13 bar using a Micromeritics ASAP 2420 volumetric adsorption analyzer with the same degassing procedure.

Isosteric Heats of Sorption. Heats of adsorption were determined from hydrogen adsorption isotherms up to a pressure of 1.13 bar at both liquid nitrogen (77.3 K) and argon (87.2 K) temperatures using a Micromeritics ASAP 2420 instrument[10] and the standard calculation routines in the Datamaster offline data reduction software (Micromeritics).

(14) Weder, C. *Angew. Chem., Int. Ed.* **2008**, *47*, 448–450.
(15) Jiang, J. X.; Su, F.; Niu, H. J.; Wood, C. D.; Campbell, N. L.; Khimyak, Y. Z.; Cooper, A. I. *Chem. Commun.* **2008**, 486–488.
(16) Dawson, R.; Su, F.; Niu, H.; Wood, C. D.; Jones, J. T. A.; Khimyak, Y.; Cooper, A. I. *Macromolecules* **2008**, *41*, 1591–1593.
(17) (a) Moroni, M.; Lemoigne, J.; Luzzati, S. *Macromolecules* **1994**, *27*, 562–571. (b) Weder, C.; Wrighton, M. S.; Spreiter, R.; Bosshard, C.; Gunter, P. *J. Phys. Chem.* **1996**, *100*, 18931–18936.
(18) (a) Weder, C.; Wrighton, M. S. *Macromolecules* **1996**, *29*, 5157–5165. (b) Babudri, F.; Colangiuli, D.; Di Bari, L.; Farinola, G. M.; Omar, O. H.; Naso, F.; Pescitelli, G. *Macromolecules* **2006**, *39*, 5206–5212.
(19) Kobayashi, N.; Kijima, M. *J. Mater. Chem.* **2007**, *17*, 4289–4296.
(20) Mendez, J. D.; Schroeter, M.; Weder, C. *Macromol. Chem. Phys.* **2007**, *208*, 1625–1636.
(21) (a) Peng, Z. H.; Pan, Y. C.; Xu, B. B.; Zhang, J. H. *J. Am. Chem. Soc.* **2000**, *122*, 6619–6623. (b) Pan, Y. C.; Lu, M.; Peng, Z. H.; Melinger, J. S. *J. Org. Chem.* **2003**, *68*, 6952–6958.
(22) Atas, E.; Peng, Z. H.; Kleiman, V. D. *J. Phys. Chem. B* **2005**, *109*, 13553–13560.
(23) Trumbo, D. L.; Marvel, C. S. *J. Polym. Sci., Part A: Polym. Chem.* **1986**, *24*, 2311–2326.

(24) Since completing this series of experiments, we have found that significantly lower Pd catalyst concentrations can be used while obtaining very similar surface areas and pore properties in the resulting polymers. For example, CMP-1 was prepared using [Pd] (1.0 mol %) to give an apparent BET surface area of 864 m²/g. This also decreases substantially the amount of Pd entrained in the polymer (see the discussion regarding H₂ isosteric heats for CMP-0−CMP-5).
(25) See the Supporting Information for full synthetic details for all networks, as well as details on the influence of the monomer concentration and monomer ratio upon the surface area (CMP-1−CMP-4), plus solid-state ¹³C{¹H} MAS NMR for CMP polymers and H₂ sorption isotherms for networks CPN-1−CPN-6.

Table 1. Series of Five PAE Networks with Increasing Average Strut Lengths

	Ethynyl monomer	Halogen monomer	Ethynes in strut	Benzenes in strut	S_{BET} (m²/g)[b]	S_{micro} (m²/g)[c]	V_{total} (cm³/g)[d]	V_{micro} (cm³/g)[e]	$I_{av (strut)}$ (nm)[f]	$I_{av (cluster)}$ (nm)[g]
CMP-0			1	1	1018 (898)	702	0.56	0.38	0.82	6.3
CMP-1[a]			2	1	834 (728)	675	0.47	0.33	1.11	6.6
CMP-2[a]			2	2	634 (562)	451	0.53	0.25	1.53	7.0
CMP-3[a]			2	3	522 (409)	350	0.26	0.18	1.90	7.5
CMP-5			2	4	512 (361)	257	0.47	0.16	2.55	7.6

[a] Data from ref 12. [b] Surface area calculated from the N_2 adsorption isotherm using the BET method. The number in parentheses is the Langmuir surface area calculated from the H_2 adsorption isotherm by application of the Langmuir equation. [c] Micropore surface area calculated from the N_2 adsorption isotherm using the t-plot method. [d] Total pore volume at $P/P_0 = 0.99$. [e] Micropore volume derived using the t-plot method based on the Halsey thickness equation. [f] Average node-to-node strut length (measured between connected quaternary carbons) derived from polymer fragment models. [g] Average overall fragment diameter derived from polymer fragment models.

Solid-State NMR. Solid-state NMR spectra were measured on a Bruker Avance 400 DSX spectrometer operating at 100.61 MHz for ^{13}C and 400.13 MHz for ^1H. $^1H–^{13}C$ cross-polarization magic angle spinning (CP/MAS) NMR experiments were carried out at an MAS rate of 10.0 kHz using zirconia rotors 4 mm in diameter. The ^1H $\pi/2$ pulse was 3.3 μs, and two-pulse phase modulation (TPPM) decoupling[26] was used during the acquisition. The Hartmann–Hahn condition was set using hexamethylbenzene. The spectra were measured using a contact time of 2.0 ms and a relaxation delay of 10.0 s. Typically 2048 scans were accumulated. The $^1H–^{13}C$ dipolar dephasing spectra were recorded at an MAS rate of 10 kHz and using dephasing delays of 20, 50, 100, and 200 μs. The variable contact time $^1H–^{13}C$ CP/MAS NMR spectra were measured using $t_m = 0.02–12.0$ ms. The $^{13}C\{^1H\}$ MAS NMR spectra were measured at an MAS rate of 10.0 kHz using TPPM decoupling. The ^{13}C $\pi/2$ pulse was 3.5 μs. The spectra were measured using a recycle delay of 30.0 s. Typically, 1024 scans were accumulated. The values of the chemical shifts are referred to that of TMS. The analysis of the spectra (deconvolution and integration) was carried out using Bruker TOPSPIN software.

Atomistic Simulations. Molecular models for the network fragments were generated using the Materials Studio Modeling 4.0 package (Accelrys Inc., San Diego, CA, 2005). The fragments were constructed by adding the repeating unit for each system in a stepwise manner. All models fully relaxed using the Discover molecular mechanics and dynamics simulation module with the

COMPASS force field.[10,27] A seed molecule was constructed for each system by fully substituting the 1,3,5-benzene node monomer with three of the corresponding linear connecting monomers. Each model was built to have an average number molar mass in the region of 11120–11210 g/mol. Any terminal halogen atoms on the periphery of the fragments were replaced with hydrogen atoms for clarity.

Results and Discussion

Effect of the Monomer Strut Length on the Pore Structure. We showed in a preliminary paper[12] that the pore structure for a series of three PAE networks could be varied by changing the length of the rigid connecting strut, much as for crystalline MOFs and COFs,[1–6] even though these PAE networks were amorphous. In this study, we extend this concept by synthesizing networks with shorter (CMP-0) and longer (CMP-5) struts (Table 1). All five polymer networks were designed to have a three-dimensional net structure arising from the three-pronged aryleneethynylene linkages (Scheme 1). As shown in Scheme 1, CMP-1 and CMP-4 had the same notional repeat unit structure but CMP-1 was produced from 1,3,5-triethynylbenzene and 1,4-diiodobenzene ($A_3 + B_2$), whereas CMP-4 was produced from 1,3,5-tribromobenzene and 1,4-ethynylbenzene ($A_2 + B_3$); as such, these materials are topologically identical but produced by two different routes. All polymerization reactions were

(26) Bennett, A. E.; Rienstra, C. M.; Auger, M.; Lakshmi, K. V.; Griffin, R. G. *J. Phys. Chem.* **1995**, *103*, 6951–6958.

(27) Sun, H. *J. Phys. Chem. B* **1998**, *102*, 7338–7364.

Scheme 1. Representative Molecular Structures for Networks CMP-0–5[a]
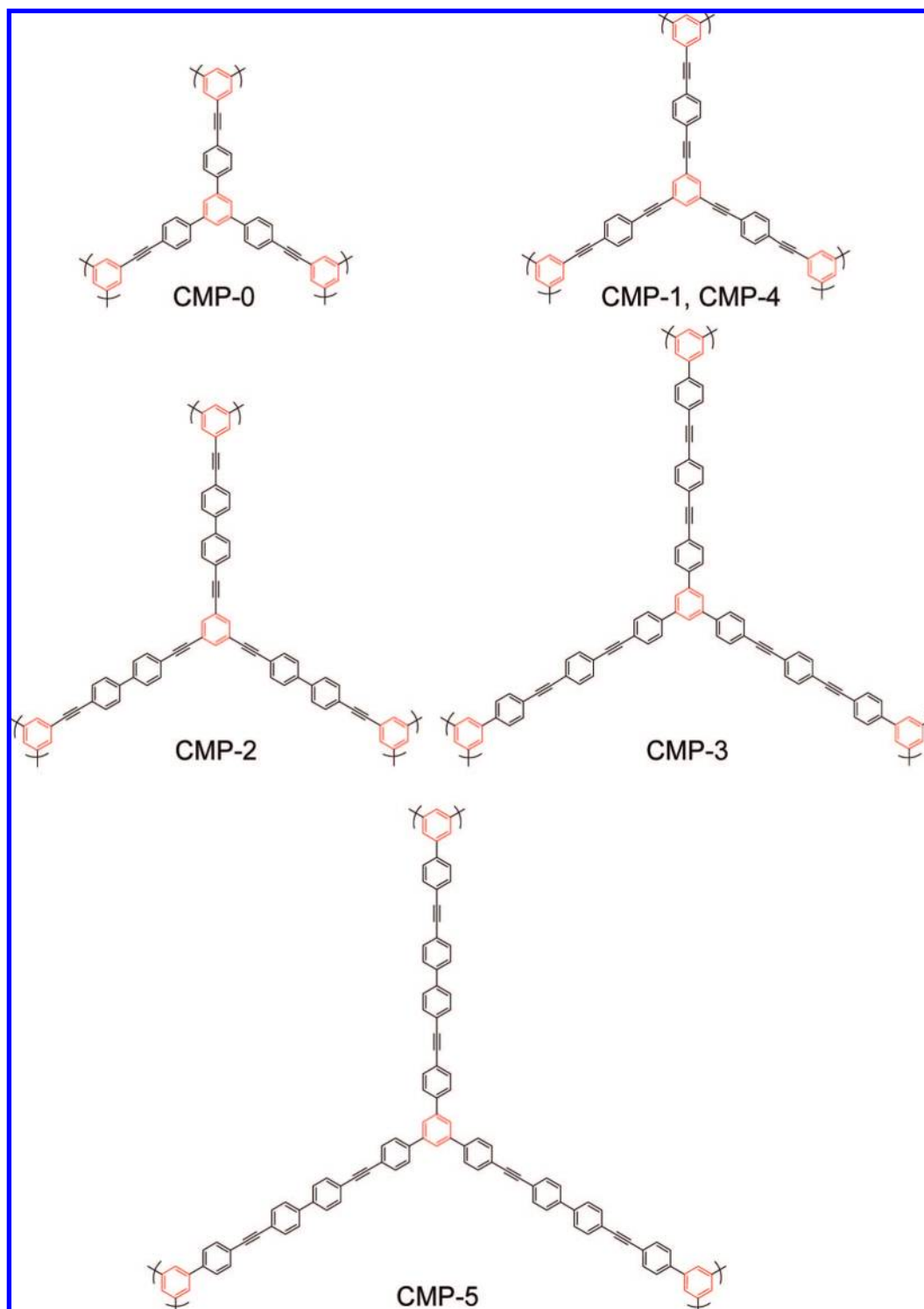
[a] The benzene "nodes" in the networks (derived from the trifunctional A_3 or B_3 monomer in each case) are shown in red.

carried out at a fixed molar halogen monomer concentration (400 mmol/L), a fixed reaction temperature (80 °C), and a reaction time of 72 h. It was found that the surface area and pore size distribution for these networks were relatively unaffected even by large changes (×10) in the monomer concentration (Supporting Information, Table S1 and Figure S1). This contrasts with macroporous vinyl polymers, for example, where surface areas can be very sensitive to even small changes in monomer concentration.[28,29] This is consistent with a mi-

croporous network where the pore dimensions are controlled primarily by the molecular structure of the network, rather than by phase behavior and phase separation.[28] The molar ratio of ethynyl to halogen functionalities in this "strut length series" was fixed at 1.5:1 since maximum surface areas and H_2 uptakes were observed consistently at this molar ratio (see also the Supporting Information, Table S2).

All polymers in the series were characterized at the molecular level by $^1H–^{13}C$ CP/MAS NMR, and the assignment of the
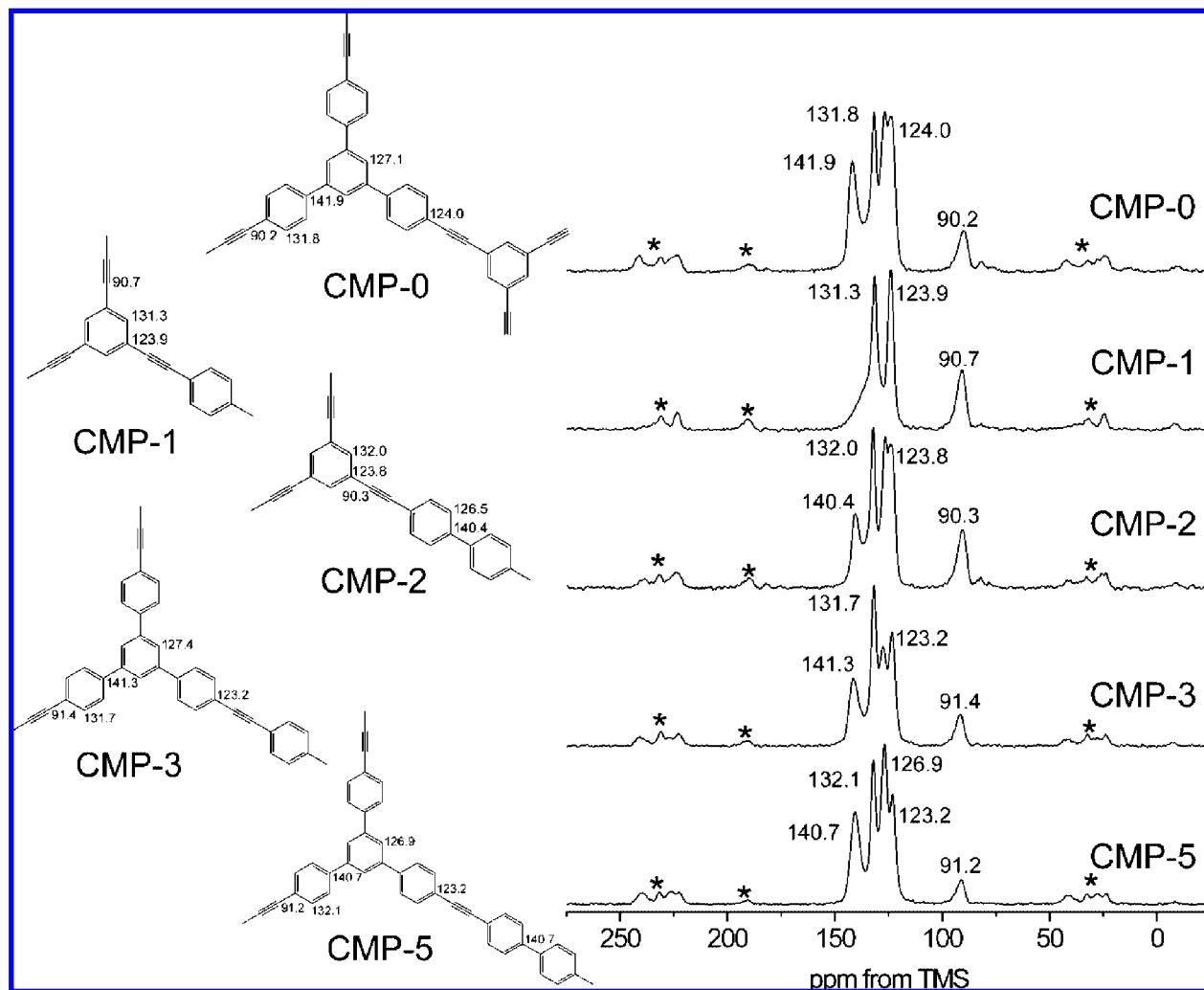
Figure 1. Solid-state $^1H-^{13}C$ CP/MAS NMR spectra for conjugated microporous PAE networks recorded at an MAS rate of 10 kHz. Asterisks denote spinning sidebands.

resonances (Figure 1) was confirmed using $^1H-^{13}C$ CP/MAS kinetics and dipolar dephasing experiments. The low-intensity lines at ca. 76 and 82 ppm can be ascribed to $-C\equiv CH$ end groups (the line at 82 ppm corresponds to the quaternary acetylene carbons). The end group content was found to be lower in the polymers produced from 1,4-ethynylbenzene (CMP-3) and 4,4′-diiodobiphenyl (CMP-5), possibly because these longer struts give rise to a greater degree of overall conformational freedom, which allows more efficient linking (i.e., fewer unreacted end groups) in the resulting network. The ratio of the intensities of the acetylenic and aromatic peaks was calculated using variable contact time $^1H-^{13}C$ CP/MAS NMR spectra as follows: CMP-0, 0.12 (expected value 0.18); CMP-1, 0.27 (expected value 0.40); CMP-2, 0.18 (expected value 0.25); CMP-3, 0.10 (expected value 0.18); CMP-5, 0.08 (expected value 0.14). These values were verified using $^{13}C\{^1H\}$ MAS NMR spectra.[25] This trend follows the expected values in accordance with the nominal structural formulae presented in Scheme 1, calculated assuming a complete condensation of $-C\equiv CH$ groups and ideal stoichiometry of the resulting polymeric frameworks. The higher than predicted content of aromatic groups indicates that these linkages are likely to be the dominant chain ends in the polymer network. The spectrum of CMP-1 shows a broad shoulder at ca. 137 ppm which may originate from the protonated carbons of aromatic end groups

bearing residual iodine atoms. The relative intensities of the peaks for all samples are consistent with their proposed formulae, although it should be noted that the accurate determination of populations of different sites is hampered by both the similarity of chemical shifts for sites in different monomers and the significant overlap of lines in the spectra of the polymer networks. A more detailed analysis of the dynamic and structural heterogeneities of these materials using advanced solid-state NMR methodology is in progress. These insoluble networks have some similarities to soluble hyperbranched polymers, and more quantitative NMR data should allow the degree of branching to be calculated.

The porous structure of this series of PAE networks was investigated by gas sorption analysis using N_2 and H_2. Figure 2a shows the N_2 adsorption and desorption isotherms for the resulting polymers, vertically offset for clarity. All networks gave rise to type I N_2 gas sorption isotherms according to IUPAC classifications.[30] The apparent BET surface area for

(28) Sherrington, D. C. *Chem. Commun.* **1998**, 2275–2286.
(29) (a) Cooper, A. I.; Holmes, A. B. *Adv. Mater.* **1999**, *11*, 1270–1274. (b) Hebb, A. K.; Senoo, K.; Bhat, R.; Cooper, A. I. *Chem. Mater.* **2003**, *15*, 2061–2069.
(30) Sing, K. S. W.; Everett, D. H.; Haul, R. A. W.; Moscou, L.; Pierotti, R. A.; Rouquerol, J.; Siemieniewska, T. *Pure Appl. Chem.* **1985**, *57*, 603–619.
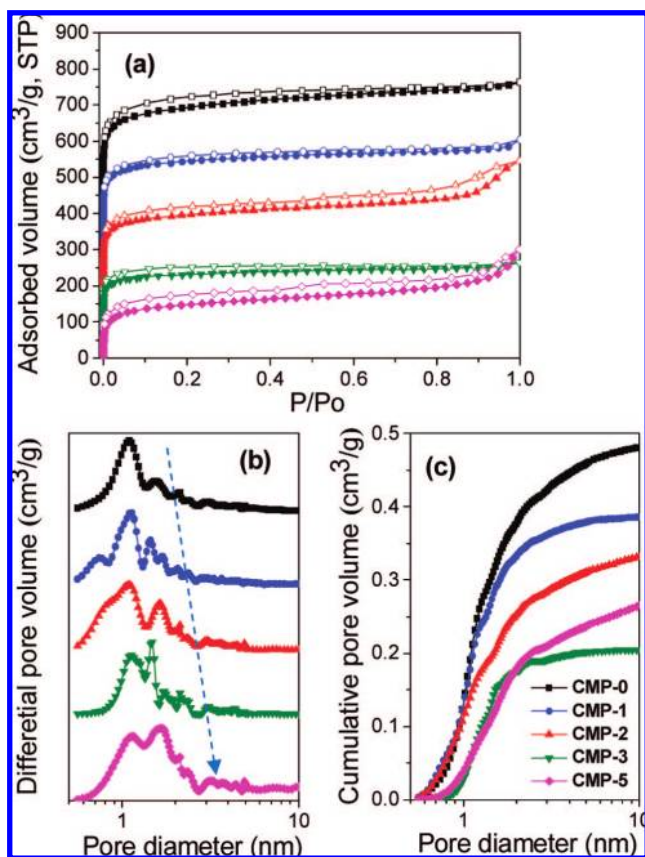
Figure 2. (a) N_2 adsorption–desorption isotherms measured at 77.3 K (the adsorption branch is labeled with filled symbols). For clarity, the isotherms of CMP-0, CMP-1, CMP-2, and CMP-3 were shifted vertically by 400, 300, 200, and 100 cm^3/g, respectively. (b) NL-DFT pore size distribution curves. The dashed arrow indicates the shift to larger average pore size in this series. (c) Cumulative pore volume curve calculated by application of NL-DFT.

these networks varied between 512 m^2/g (CMP-5) and 1018 m^2/g (CMP-0). The small rise in the N_2 uptake at high relative pressures ($P/P_0 > 0.8$) in the adsorption isotherms for CMP-2 and CMP-5 may stem from interparticulate porosity associated with the meso- and macrostructures of the samples. Figure 2b shows pore size distribution curves for the five CMP networks using the nonlocal density functional theory (NL-DFT). In general, the micropore size distribution is shifted systematically to larger pore diameters for the series CMP-0–CMP-5 as the monomer strut length is increased, and the overall micropore volume also falls (from 0.38 to 0.16 cm^3/g) over this series. This is illustrated in the NL-DFT cumulative pore volume plots for the five networks (Figure 2c). In particular, CMP-3 and CMP-5, which were formed using longer struts (Scheme 1, Table 1) exhibit almost no ultramicropore volume below a pore diameter of about 0.9 nm. The observations for CMP-0 and CMP-5 are consistent with our previous results[12] and further illustrate that micropore dimensions and surface areas can be tuned synthetically by varying the monomer strut length. For example, CMP-0 (which has the shortest struts in this series) has an apparent BET surface area (1018 m^2/g) which is higher than that of CMP-1 or any of the other networks reported in our preliminary paper.[12] The polymer CMP-4, which was topologically equivalent to CMP-1, exhibited porous properties ($S_{BET} = 744$ m^2/g, $S_{micro} = 596$ m^2/g, $V_{total} = 0.39$ cm^3/g, $V_{micro} = 0.29$ cm^3/g) which were very similar to those of CMP-1, although it was produced by a different route. Compared to

CMP-1, CMP-4 had a slightly lower surface area; this may be a result of the lower reactivity of aryl bromides with respect to aryl iodides in Pd/Cu-catalyzed cross-coupling reactions. In general, we have found that, all other things being equal, iodine-substituted monomers give rise to slightly higher surface area PAE materials.

Atomistic simulations were used to build representative fragments for each of the five networks. Each fragment was built to have a similar molar mass (between 11 120 and 11 210 g/mol). We believe that the amorphous three-dimensional structure of these PAE networks arises from the bending of the struts out of plane of the benzene nodes, from the dihedral angle between struts on adjacent connected nodes, from bending of the struts themselves, and from in-plane deviation of the angle between struts from the hypothetical 120° imposed by the 1,3,5-substituted node geometry. CMP-0 has the shortest strut length of 0.82 nm. However, the presence of the 1,3,5-triphenyl-substituted benzene node leads to a broadened distribution range of in-plane and out-of-plane bending angles (103–131° and 3–57°, respectively). CMP-1, while having a longer average strut length of 1.11 nm, has the most geometrically simple structure: the out-of-plane bending of struts ranges from 0° to 10°, while in-plane angles range from 115° to 130°. The greatest flexibility is seen for the simulation of CMP-5, which contains both biphenyl moieties and the 1,3,5-triphenyl-substituted benzene node. This model also has the longest strut length, $L_{av(strut)}$, of 2.550 nm. The in-plane and out-of-plane bending angles in this model range between 70° and 143° and between 26° and 95°, respectively.

Figure 3 shows cluster fragments for CMP-0–CMP-5 derived from these molecular models. The overall average fragment diameter, $L_{av(cluster)}$ in Table 1, increases in the series CMP-0–CMP-5 in keeping with the increase in the average strut length, $L_{av(strut)}$. The increased degree of conformational freedom in the extended struts in this series of models allows for greater intramolecular intercalation and space-filling within the fragments, and hence, the increase in cluster size does not scale in direct proportion to the average strut length. We believe that this conformational freedom may also contribute to the reduction in micropore volume for the networks with longer struts (Table 1). These models represent *fragments* of the networks rather than the pore structure itself. It is likely, for example, that there is significantly more intermolecular catenation and entanglement of fragments in the actual samples, consistent with the fact that these fragment models significantly overestimate the micropore volume in comparison with measured values. The hydrogen sorption properties of the polymers were also investigated by volumetric methods.[9,10] Figure 4 shows the H_2 adsorption isotherms for the PAE networks at 77.3 K, up to a maximum H_2 pressure of 1.13 bar. CMP-0 has the smallest strut length, the highest micropore volume, and the highest apparent BET surface area, and this sample exhibited the largest H_2 uptake (155 cm^3/g, ~1.4 wt %; approximately 215 cm^3/g at 8 bar of H_2). CMP-5 showed the lowest H_2 uptake (67 cm^3/g, ~0.6 wt %). In general, there was a systematic change in H_2 uptake as a function of molecular strut length in the polymers (Figure 4). These results can be explained by the fact that ultramicropores, rather than "large" micropores or mesopores, contribute mostly to H_2 adsorption at this pressure and temperature; as such, H_2 is a sensitive probe for the variation in micropore structure in this series. The H_2 uptake per unit BET surface area (as calculated by N_2 sorption) for these PAE networks is significantly greater than observed for our highest surface area hyper-
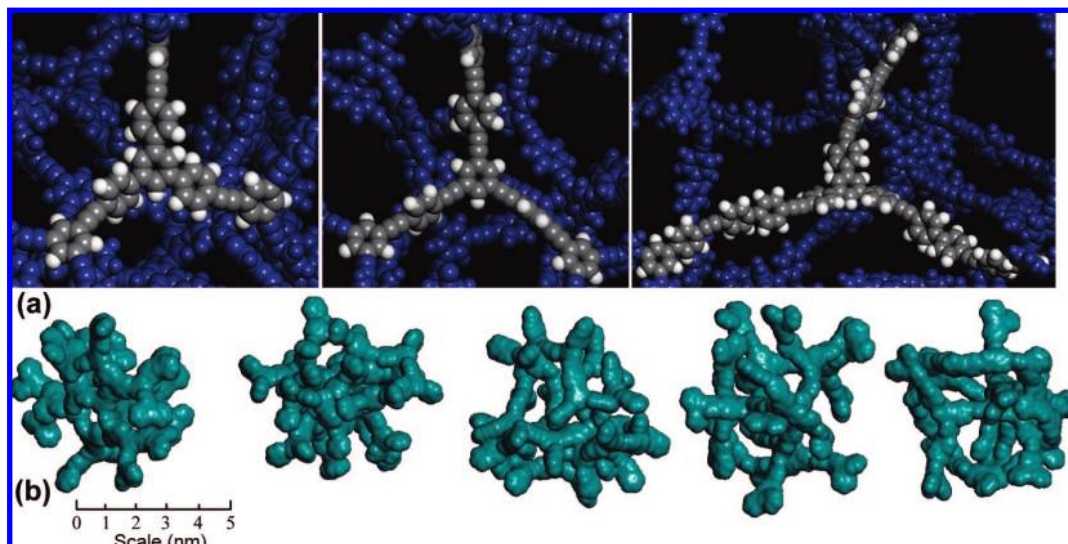
Figure 3. Atomistic simulations for PAE networks with different strut lengths. (a) Node−strut topology for simulated network fragments for CMP-0 (left), CMP-1 (center), and CMP-5 (right). A single 1,3,5-connected benzene node connecting three other nodes via rigid struts is highlighted (in gray/white) in each case. (b) Atomistic simulations of network fragments for CMP-0, CMP-1, CMP-2, CMP-3, and CMP-5 (left to right). The solvent-accessible surface is shown (in green) in each case, as calculated using a solvent diameter of 0.182 nm. Each model was built to have an average number molar mass in the range 11120−11210 g/mol.
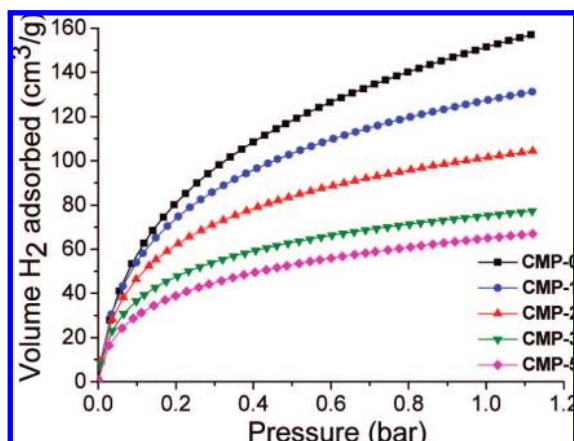
Figure 4. Volumetric H_2 adsorption isotherms for CMP-0−5 at 77.3 K.

cross-linked polymers[10] under equivalent conditions (e.g., 1.36 × 10^{-5} g of H_2/m^2 for CMP-0 versus 8.46 × 10^{-6} g of H_2/m^2 for hyper-cross-linked polymer **43**).[10] Similarly, the H_2 sorption per unit micropore volume for CMP-0 is about 20% higher than for **43** (3.63 × 10^{-2} and 2.98 × 10^{-2} g/cm^3, respectively).

The isosteric heat of sorption for H_2 on these PAE materials was calculated as a function of H_2 coverage from comparison of the adsorption isotherms at 77.3 and 87.2 K (Figure 5).[10,31] All five networks exhibited low gas coverage enthalpies of adsorption of ∼10 kJ/mol, falling to between 4 and 8 kJ/mol with increasing H_2 coverage. In general, these isosteric heats are higher than we observed for hyper-cross-linked polymers.[10] The initial isosteric heats at low H_2 coverage for the PAE networks are comparable to the highest reported for MOFs,[32] despite the fact that these polymers do not contain charged metal
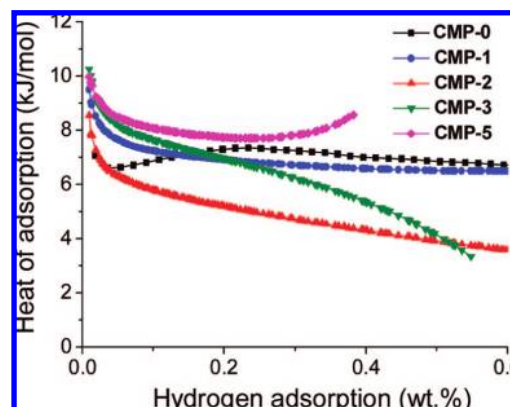
**Figure 5.** Isosteric heats of sorption for H_2 on networks CMP-0−5.

centers.[33] The isosteric heats at higher H_2 coverages for networks such as CMP-5 are comparable to values reported recently by Svec and colleagues for hyper-cross-linked polyanilines.[11] A preponderance of small ultramicropores (<0.7 nm) might in principle give rise to multiwall interactions and enhanced isosteric heats for H_2, but no simple correlation was observed between the average pore size and isosteric heat for these materials. In fact, CMP-5 − which had the largest average micropore size − exhibited the highest overall isosteric heat. It should be noted, however, that these materials vary in both chemical structure (Scheme 1) *and* average micropore size and do not in this respect form a fully homologous series. A number of factors other than pore size may influence isosteric heats. First, these materials contain small, variable quantities of residual palladium, copper, and iodine (typically <1 atom % for each element).[25] Species such as Pd could certainly influence H_2 sorption, but we did not find any clear correlation between the quantity of residual Pd, Cu, or I and the average isosteric heat (Supporting Information, Figure S3). Second, ethynyl end groups are present in these networks, and it was noted, for example,

(31) (a) Dincă, M.; Yu, A. F.; Long, J. R. *J. Am. Chem. Soc.* **2006**, *128*, 8904–8913. (b) Rowsell, J. L. C.; Yaghi, O. M. *J. Am. Chem. Soc.* **2006**, *128*, 1304–1315.
(32) Dincă, M.; Long, J. R. *J. Am. Chem. Soc.* **2007**, *129*, 11172–11176.

(33) Panella, B.; Hönes, K.; Müller, U.; Trukhan, N.; Schubert, M.; Pütter, H.; Hirscher, M. *Angew. Chem., Int. Ed.* **2008**, *47*, 2138–2142.
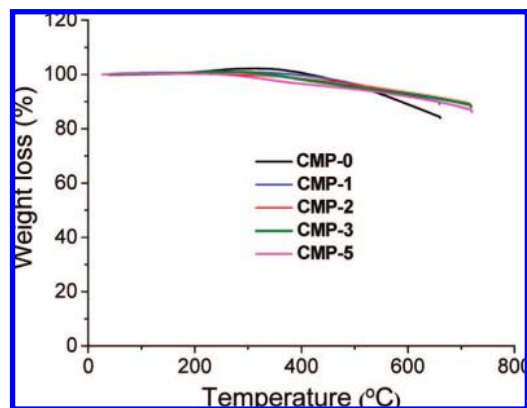
Figure 6. Thermogravimetric analysis for PAE networks CMP-0−CMP-5. The heating rate is 5 °C/min under nitrogen.

that the two polymers with the highest low-coverage isosteric heats (CMP-5 and CMP-3) appeared to have lower −C≡CH end group concentrations (see the NMR discussion above). One cannot infer from these data alone, however, that this is a dominant factor. Third, the various networks in this series have different electronic conjugation patterns and varying alternation of benzene and alkyne functionalities (Scheme 1). Second-order Møller−Plesset calculations for small aromatics and fused-ring systems[34] have suggested that the interaction energy between H_2 and benzene π-systems is affected by the degree of conjugation and also by the presence of substituents. For example, extended conjugation (coronene versus benzene) led to enhanced H_2−arene interactions.[34] For monosubstituted benzenes such as cyanobenzene or fluorobenzene, H_2 was found to interact preferentially with the center of the aromatic ring in an end-on fashion.[34] As such, the presence of ethynyl or halogen end groups in our polymers might influence interactions with H_2, either directly as substituents or because these groups are indicative of a lower degree of cross-linking and, thus, a reduction in extended electronic conjugation. It is therefore very hard at this time to fully deconvolute the potential effects on the isosteric heat of the pore size distribution, chemical functionality, and electronic conjugation for these materials.

These porous PAE networks were found to have good chemical and thermal stability and did not require any special handling to maintain microporosity. The workup procedure involved multiple washing steps in air followed by extended Soxhlet extraction. The polymers were also stable toward water; indeed, no change in surface area was observed when the materials were treated with aqueous solutions of acid or base. By contrast, MOFs and COFs can vary in stability from being highly air sensitive to being quite robust.[1–6] In general, however, the coordinate bonding which allows the broad structural diversity in crystalline MOFs and COFs may not in general be compatible with harsher physical conditions, such as acidic and basic environments, and hence, these PAE materials may offer some advantages in such applications. The microporous PAE networks were also found to have good thermal stability as a result of their cross-linked structure and strong covalent bonds. The polymers showed little thermal decomposition under nitrogen gas below temperatures of around 400 °C (Figure 6).

Controlling the Micropore Size and Surface Area by Statistical Copolymerization. A well-known advantage of organic polymers is the ability to produce copolymers over a continuous range of relative monomer compositions and hence achieve systematic control over material properties such as glass transition temperature, melting temperature, solubility, and pH response. Statistical copolymerization has not until now been used to fine-tune the micropore size in materials. Here, the amorphous nature of these PAE systems is an advantage. While pore properties in MOFs and COFs have been varied systematically by changing the connecting ligands,[1–6] the structures are "quantized" in terms of the unit of variation, for example, the difference in length between ligands in a series of materials. As such, the gradations between structures in a series may be small but are nevertheless finite, and this strategy requires that each ligand in the series reacts in a similar way to form a stable, crystalline porous structure. Similarly, while MOF "copolymers" have been prepared using more than one connecting ligand,[35] the physical properties of the materials are a result of the accessible thermodynamically stable crystal structures and are not *continuously* variable as a function of the relative ligand ratio. By contrast, it should be possible to "tune" properties such as micropore size and surface area in amorphous PAE networks in a completely continuous fashion, such that the degree of fine control over these properties is limited only by the inherent variability in the polymerization process itself. To test this idea, we synthesized a series of copolymers of 1,3,5-triethynylbenzene with 1,4-diiodobenzene and/or 4,4′-diiodobiphenyl (CPN-1−6; Table 2, Scheme 2). In principle, the average micropore size and surface area would be expected to increase systematically as the percentage of the shorter monomer strut, 1,4-diiodobenzene, is increased.

To check that the two comonomers had similar reactivities, the relative monomer incorporation in the networks was investigated by solid-state NMR spectra (Figure 7). The ¹H−¹³C CP/MAS solid-state NMR spectra for the CPN networks confirmed the presence of two different types of building units in the copolymers. The intensity of the peaks at 140.4 and 126.1 ppm, which are characteristic of the 4,4′-diiodobiphenyl monomer, increased systematically with its content in the initial monomer feed.

The BET surface areas for these networks were found to decrease from 856 m²/g for CPN-1 to 643 m²/g for CPN-6, as measured by nitrogen sorption. Figure 8a shows the full nitrogen adsorption and desorption isotherms for the six copolymer networks. All of the copolymers gave rise to type I gas sorption isotherms, indicating that all of the materials were microporous. Figure 8b shows the NL-DFT pore size distribution curves for the six networks. The micropore size distribution is shifted to larger pore diameters for the series of networks from CPN-1 to CPN-6 as the ratio of the longer strut monomer, 4,4′-diiodobiphenyl, increases. This is shown by the NL-DFT cumulative pore volume plots for these networks (Figure 8c). Even though

(34) Hübner, O.; Glöss, A.; Fichtner, M.; Klopper, W. *J. Phys. Chem. A* **2004**, *108*, 3019–3023.
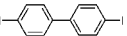
(35) (a) Wang, C. C.; Kuo, C. T.; Yang, J. C.; Lee, G. H.; Shih, W. J.; Sheu, H. S. *Cryst. Growth Des.* **2007**, *7*, 1476–1482. (b) Wang, C. C.; Tseng, S. M.; Lin, S. Y.; Liu, F. C.; Dai, S. C.; Lee, G. H.; Shih, W. J.; Sheu, H. S. *Cryst. Growth Des.* **2007**, *7*, 1783–1790. (c) Yang, E. C.; Zhao, H. K.; Ding, B.; Wang, X. G.; Zhao, X. J. *Cryst. Growth Des.* **2007**, *7*, 2009–2015.
(36) (a) Deng, W. Q.; Xu, X.; Goddard, W. A. *Phys. Rev. Lett.* **2004**, *92*, No. 166103. (b) Lee, H.; Choi, W. I.; Ihm, J. *Phys. Rev. Lett.* **2006**, *97*, No. 056104.
(37) Cooper, A. I.; Poliakoff, M. *Chem. Commun.* **2007**, 2965–2967.
(38) Trewin, A.; Darling, G. R.; Cooper, A. I. *New J. Chem.* **2008**, *32*, 17–20.

Table 2. Copolymerization with Different Molar Ratios of Two Halogen Monomers[a]

			S_{BET} (m^2/g)[b]	S_{micro} (m^2/g)[c]	V_{total} (cm^3/g)[d]	V_{micro} (cm^3/g)[e]	H_2 uptake (wt. %)[f]
CPN-1	100	0	856 (726)	665	0.53	0.32	1.14
CPN-2	80	20	775 (710)	584	0.42	0.31	1.09
CPN-3	60	40	757 (669)	580	0.39	0.30	1.07
CPN-4	40	60	749 (638)	576	0.40	0.29	1.04
CPN-5	20	80	722 (575)	526	0.39	0.29	0.95
CPN-6	0	100	643 (556)	504	0.46	0.25	0.92

[a] All reactions were carried out under a monomer concentration of 400 mmol/L, 80 °C/72 h. [b] Surface area calculated from the N_2 adsorption isotherm using the BET method. The number in parentheses is the Langmuir surface area calculated from the H_2 adsorption isotherm by application of the Langmuir equation. [c] Micropore surface area calculated from the N_2 adsorption isotherm using the t-plot method. [d] Total pore volume at P/P_0 = 0.99. [e] Micropore volume derived using the t-plot method based on the Halsey thickness equation. [f] Data were obtained at 1.13 bar and 77.3 K.

Scheme 2. Synthetic Route of Copolymerization for CPN-1−6
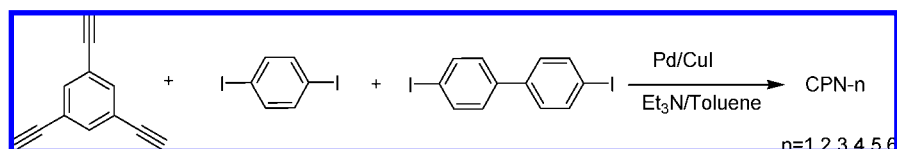
the changes in the cumulative curves are small (particularly for CPN-2−CPN-4), the shift is systematic and all six cumulative curves fall in the predicted order. Likewise, the hydrogen adsorption isotherms for the six copolymers (Supporting Infor-


Figure 7. Solid-state $^1H-^{13}C$ CP/MAS NMR spectra for conjugated microporous CPN networks recorded at an MAS rate of 10 kHz. Asterisks denote spinning sidebands.

mation, Figure S4) followed the same trend and order, again suggesting that H_2 uptake is a sensitive probe for the micropore surface area in materials of this type. The systematic variation in surface area for these PAE materials as a function of comonomer ratio is shown in Figure 9. These data also illustrate the high reproducibility of these polymerization reactions: networks CPN-1 and CPN-6 are repeats of CMP-1 and CMP-2, respectively, and both the BET surface areas and H_2 isotherm Langmuir surface areas differ by less than ±3% for the two pairs of samples (cf. Tables 1 and 2). In effect, this series of CPN copolymers corresponds to the materials that lie "between" networks CMP-1 and CMP-2 in the aforementioned strut-length series, as illustrated graphically in Figure 9 (also cf. Figures 2c and 8c). This demonstrates the essentially continuous synthetic variation that can be achieved in terms of micropore size and surface area, at least within the apparent ±3% reproducibility of the system, and we believe that this degree of direct, continuous synthetic control is unprecedented for any microporous material.

While control over surface area and pore size was very good, the isosteric heat of sorption for H_2 was found, as for the CMP series, not to fall into a simple, rational order (Supporting Information, Figure S5). For example, we did not observe the isosteric heat to simply increase with decreasing pore size. Also, the isosteric heat for CNP-1 was found to be slightly lower than observed for CPN-6, which is the reverse trend observed for the corresponding samples CMP-1 and CMP-2. Again, this suggests that variability at the molecular level may be dominating. It should be stressed however that these differences are relatively small (low-coverage heats for the whole CPN series vary between 6.0 and 7.5 kJ/mol) and that all of these energies are much too low, for example, to allow close-to-ambient-temperature H_2 sorption.

These PAE materials, for example, CMP-0, exhibit apparent BET surface areas that are higher than or equal to
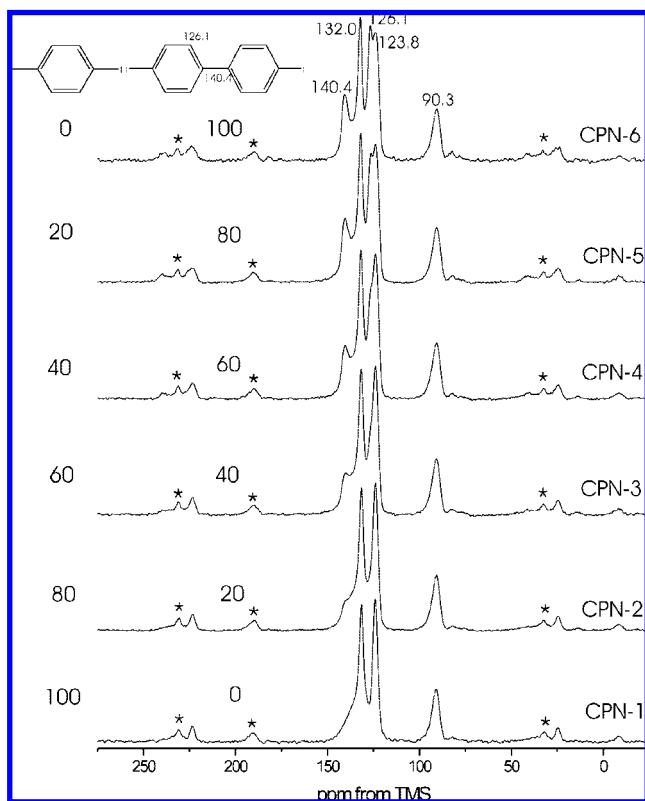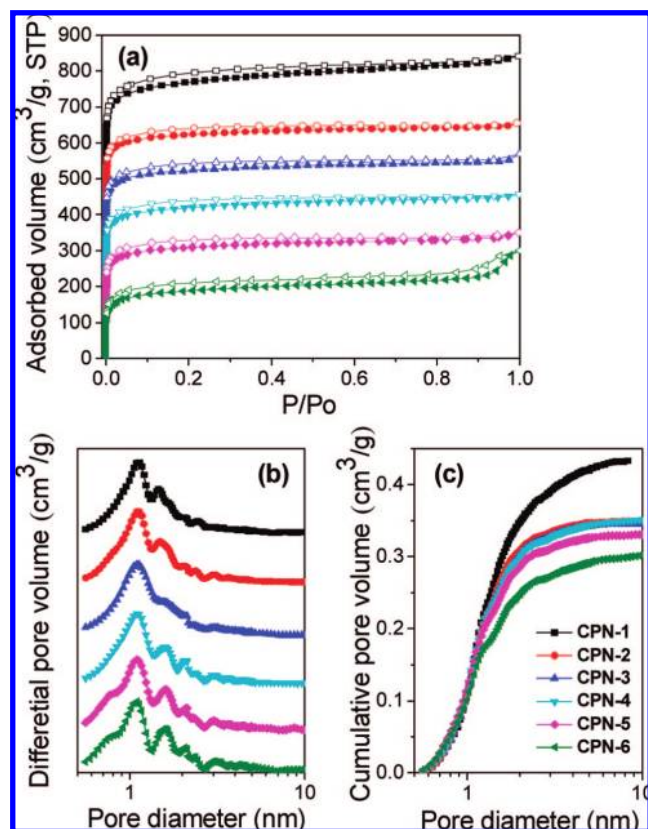
Figure 8. (a) N_2 adsorption−desorption isotherms measured at 77.3 K (the adsorption branch is labeled with filled symbols, and the desorption branch is labeled with empty symbols). For clarity, the isotherms of CPN-1, CPN-2, CPN-3, CPN-4, and CPN-5 were shifted vertically by 500, 400, 300, 200, and 100 cm^3/g, respectively. (b) Pore size distribution curves. (c) NL-DFT cumulative pore volume curve.
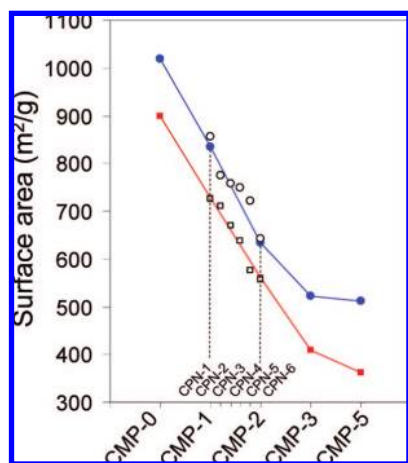
Figure 9. Surface area as a function of polymer structure for polymers CMP-1−CMP-5 (closed symbols) and copolymers CPN-1−CPN-6 (open symbols). Both the apparent N_2 BET surface area (circles) and the Langmuir surface area (as calculated from the H_2 adsorption isotherm, squares) are shown. The series of CPN copolymers falls between the respective homopolymers, CMP-1 and CMP-2, for both the N_2 and H_2 sorption measurements.

those of most microporous organic polymers,[7,28,29] although substantially lower than those observed for some hyper-cross-linked materials.[8–11] Unlike hyper-cross-linked polymers, however, it is possible to fine-tune the micropore size and surface area in PAE networks by systematic variation of the monomer strut length. In this regard, PAE networks have

some similarity to MOFs[1,2] and COFs.[3–6] Indeed, CMP-1 (SA_{BET} = 834 m^2/g, S_{micro} = 675 m^2/g, pore volume 0.33 cm^3/g) exhibited a N_2 isotherm and pore size distribution (Figure 2) which were both very similar to those reported for COF-1 (SA_{BET} = 711 m^2/g, S_{micro} = 587 m^2/g, pore volume 0.32 cm^3/g).[3] The properties of CMP-2 were also similar to those of COF-1; in general, CMP-1 was somewhat more microporous than COF-1, whereas CMP-2 was somewhat less so. COF-1 is crystalline,[3] whereas CMP-1 is amorphous;[12] nevertheless, the close similarity in sorption properties may be more than superficial since both materials are composed of a rigid 1,3,5-substituted node−strut topology. Moreover, in both cases, struts and nodes may form "eclipsed" conformations—COF-1 by eclipsing of extended ordered hexagonal sheets[3] and CMP-1 by interpenetration of the amorphous polymer network fragments (see the simulation discussion above). While it is possible to continuously fine-tune the surface area and micropore size by changing the strut length for PAEs, the correspondence between "design" and structure is perhaps more indirect than observed for COFs. For example, COF-10 (with a relatively long biphenyldiboronic acid strut) was reported to be mesoporous.[5] By contrast, PAEs with extended strut lengths (CMP-2−CMP-5) showed a shift to larger average micropore sizes (Figure 2), but all networks were microporous, not mesoporous, and exhibited type I isotherms. Similarly, the pore volume for the COF series (COF-6, COF-8, COF-12) was found to increase with increasing spacer length,[5] whereas the pore volume for our PAE materials *decreases* in the series CMP-0−CMP-5. This is a fundamental difference between these two classes of material and reflects the fact that the PAE pore structure is not crystallographically defined by the monomer structure. Rather, we propose that the average pore size distribution envelope is related statistically to the average strut length and polymer topology and that the decrease in overall pore volume with increasing strut length is a consequence of greater conformational freedom and chain interpenetration, as suggested by atomistic simulations. We have exploited this, uniquely, by continuous fine-tuning of pore size distributions and surface areas via statistical copolymerization of monomers with different strut lengths (Figure 9). Our PAE materials exhibit apparent BET surface areas which are much lower than the highest reported for COFs (e.g., 4210 m^2/g for COF-103).[4] It may be very difficult to approach surface areas of this magnitude in amorphous polymers such as these without introducing new strategies: for example, molecular templating approaches to significantly enhance the creation of micropore volume. Nevertheless, PAE materials may have unique advantages as a result of combining fine control over micropore properties with very good chemical and thermal stability. These PAEs are also highly conjugated, unlike MOFs, COFs, PIMs, or hyper-cross-linked polymers. There is therefore a wealth of opportunity for producing robust microporous materials with specific functionality; for example, by attaching metals to these networks to facilitate catalysis or new electrical properties or to introduce high-binding energy sites such as metals,[36] transition-metal complexes,[37] or "naked" halides[38] for gas storage applications.

Conclusion

We have synthesized microporous conjugated PAE networks with BET surface areas of more than 1000 m^2/g and shown that the surface area and pore size can be controlled by the monomer structure. For the first time, we have shown that the

average micropore size and surface area can be fine-tuned in a continuous fashion by statistical copolymerization, something which is possible with amorphous copolymers but very difficult to achieve with crystalline materials. This may be useful in applications such as molecular separations where particular optimal pore sizes are required. These PAE networks combine some of the advantages of microporous and mesoporous carbon, for example, chemical robustness, tunable pore size,[39] and extended conjugation, with the broad synthetic versatility of organic polymers, while offering an unprecedented degree of pore size control for an amorphous microporous polymer system.

Supporting Information Available: Full synthetic details, solid-state $^{13}C\{^1H\}$ MAS NMR for CMP polymers, and H_2 sorption isotherms and isosteric heat data for networks CPN-1−CPN-6. This material is available free of charge via the Internet at http://pubs.acs.org.

JA8010176

(39) Jun, S.; Joo, S. H.; Ryoo, R.; Kruk, M.; Jaroniec, M.; Liu, Z.; Ohsuna, T.; Terasaki, O. *J. Am. Chem. Soc.* **2000**, *122*, 10712–10713.